communications materials

A Nature Portfolio journal

Article

https://doi.org/10.1038/s43246-025-01067-9

Dynamic bacterial growth modulation in structurally distinct and functionally tuneable agarose hydrogels

Check for updates

Andrea Dsouza [1], Dylan Taylor[2], Christopher Parmenter [3], Rachel A. Hand [4], Julia Brettschneider[5], Meera Unnikrishnan [1] ✉, Chrystala Constantinidou [1,6] ✉ & Jérôme Charmet [1,7,8] ✉

Bacterial adaptability to diverse environments drives infection, persistence, and antibiotic resistance. Although hydrogels are increasingly used to model such conditions, the factors governing hydrogel-dependent bacterial growth is complex. Here, we focus on agarose hydrogels and investigate how their material properties influence bacterial proliferation. Using two agarose types – hydroxyethyl substituted and unsubstituted – at varying concentrations, we tested four bacterial species (*E. coli*, *P. fluorescens*, *S. aureus*, *B. subtilis*) across five nutrient media yielding 120 conditions. Growth consistently decreased with increasing hydrogel stiffness and water loss in unsubstituted and substituted agarose hydrogels, regardless of species. Media effects were largely due to their impact on hydrogel properties rather than nutrient content. Furthermore, electrostatic repulsion between Gram positive bacteria and anionic unsubstituted agarose suppressed growth in high concentration gels. These findings demonstrate that bacterial growth in agarose systems is primarily shaped by gel mechanics and surface interactions, informing the design of infection models and antibacterial materials.

Bacteria have acquired an extraordinary ability to adapt and thrive in various microenvironments due to survival mechanisms including formation of complex biofilms[1,2], exchange of genetic material by horizontal gene transfer[3–6], and antimicrobial resistance[7,8]. Consequently, the incidence of bacterial infections, particularly antibiotic-resistant infections, is increasing faster than ever and has claimed ~4.71 million deaths globally in 2021 alone[9]. Life-threatening infections are also a major driver of significant healthcare and economic costs, and results in socio-economic devastation and heightened vulnerability in low-to-middle income countries[10–13]. The World Health Organization has declared antimicrobial resistance as one of the top global public health and development threats[14,15], highlighting the urgent need for new diagnostics and better treatments.

Due to their unique characteristics including porosity, elasticity, biocompatibility, and ease of customization, hydrogels have been extensively designed for exploring bacterial interactions, antibacterial formulations, wound dressings, and smart biosensors for bacterial detection[16–21]. Hydrogels are considered one of the most promising in vitro models for studying bacterial growth and anti-bacterial activities[16]. In particular, agarose hydrogels are valued in microbiology for their chemical inertness, structural simplicity, and widespread use in culturing and visualising bacterial cells. However, agarose offers more than routine use as a culture medium. Its chemically defined, inert backbone enables controlled tuning of stiffness, porosity, water retention, and surface charge without introducing antimicrobial effects, making it ideal for isolating material-driven influence on bacterial behaviour. Chemical substitutions such as hydroxyethylation modify these physical properties while preserving the same polysaccharide structure. Thus, comparing unsubstituted and substituted agarose provides a reductionist platform to decouple material chemistry from bacterial response. Yet, despite agarose's widespread use, the advantages and limitations of its variants as bacterial growth matrices have not been systematically assessed.

Despite growing interest in using hydrogels to understand and control bacterial behaviour, the fundamental properties that govern bacterial growth within these matrices remain poorly understood. This gap is particularly important because bacteria in real infection settings such as wound tissues, abscesses encounter soft, hydrated environments that closely

[1]Division of Biomedical Sciences, Warwick Medical School, The University of Warwick, Coventry, UK. [2]Big Data Institute, Li Ka Shing Centre for Health Information and Discovery, Nuffield Department of Population Health, University of Oxford, Oxford, UK. [3]Nanoscale and Microscale Research Centre, The University of Nottingham, Nottingham, UK. [4]Department of Chemistry, The University of Warwick, Warwick, UK. [5]Department of Statistics, The University of Warwick, Coventry, UK. [6]Bioinformatics Research Technology Platform, The University of Warwick, Warwick, UK. [7]School of Engineering - HE-Arc Ingénierie, HES-SO University of Applied Sciences Western Switzerland, Neuchâtel, Switzerland. [8]School of Precision and Biomedical Engineering, University of Bern, Bern, Switzerland. ✉e-mail: m.unnikrishnan@warwick.ac.uk; c.i.constantinidou@warwick.ac.uk; j.charmet@warwick.ac.uk

resemble hydrogels. In such environments, bacterial persistence is often linked to altered growth, physiology, and reduced antibiotic efficacy, all of which can be influenced by the nature of surrounding matrix. However, it remains unclear how specific hydrogel properties including stiffness, water availability, and surface charge, contribute to bacterial colonization and expansion in these environments.

Properties such as stiffness, porosity, hydrophilicity, and nutrient content have been implicated[22–25], but findings, particularly concerning stiffness have been inconsistent. For instance, some studies report increased bacterial growth with increased stiffness, while others observe the opposite. In agarose-based systems, Guegan et al. found that Gram-negative *Pseudoalteromonas sp.* adhered more effectively to stiffer gels, whereas *Bacillus subtilis* showed no preference[26]. Stiffer polyethylene glycol diacrylate hydrogels have also been shown to promote increased *Escherichia coli* (*E. coli*) and *Staphylococcus aureus (S. aureus)* adhesion[27]. Similarly, increased mechanical stress in stiff agarose and polyacrylamide hydrogels have been shown to enhance *Pseudomonas aeruginosa* accumulation and *Serratia marcescens* colony expansion[28,29]. However, contradictory results in other materials, such as reduced *Staphylococcus aureus* adhesion on stiffer polyacrylamide substrates, suggest that hydrogel chemistry, not stiffness alone, governs bacterial response[30,31]. Furthermore, bacterial envelope characteristics, particularly surface charge and production of extracellular polymeric substances are often underrepresented in these analyses, despite their key role in hydrogel-bacteria interactions[16,20,32].

To address this knowledge gap, our study focuses specifically on agarose hydrogels as a controllable platform to decouple and systematically investigate the physicochemical parameters that regulate bacterial growth. By determining how mechanical stiffness, hydration, and matrix charge influence species-specific proliferation, we aim to generate mechanistic insights that are relevant to bacterial colonization of soft tissue-like environments, infection persistence, and the design of antibacterial biomaterials. We used two structurally distinct agarose derivatives: (i) unsubstituted agarose (US), containing only hydroxyl (–OH) groups, and (ii) substituted agarose (S), containing hydroxyethyl ($–C_2H_5OH$) groups in addition to hydroxyls. Though derived from the same polysaccharide backbone of D-galactose and 3,6-anhydro-L-galactopyranose, these modifications confer differing mechanical and hydration properties to the gels.

To evaluate how these structural differences influence bacterial behaviour, we examined the growth of four representative bacterial species: *E. coli* and *Pseudomonas fluorescens* (Gram-negative), and *S. aureus* and *B. subtilis* (Gram-positive) across both hydrogel types. We further varied hydrogel concentration (0.2%, 0.5%, and 1%) and encapsulated each with five commonly used bacterial nutrient media including Nutrient Broth (NB), Lysogeny Broth (LB), Tryptic Soy Broth (TSB), and two formulations of Mueller Hinton Broth (M1 and M2), resulting in 120 experimental conditions (Fig. 1).

In this study, we aimed to investigate how hydrogel physicochemical properties, including stiffness, water retention, and surface charge, influence species-specific bacterial growth. Our results reveal that bacterial growth in agarose hydrogels is predominantly governed by stiffness and water loss, with growth consistently increasing in softer, more hydrated hydrogels across all species. Substituted hydrogels, which exhibit lower stiffness and reduced water loss, supported greater bacterial growth than unsubstituted counterparts. Interestingly, the effect of nutrient media was mediated more through its impact on hydrogel physical properties than direct nutrient content. Additionally, we observed that electrostatic repulsion between negatively charged bacteria and the anionic unsubstituted hydrogels inhibited growth in certain conditions, particularly at higher gel concentrations. Collectively, these findings highlight the critical role of hydrogel physicochemical properties and bacterial envelope characteristics in modulating bacterial growth behaviour within agarose-based systems. While our study is limited to agarose hydrogels, the observed species- and material-dependent variability suggests that generalizations based solely on bulk mechanical properties may be insufficient. These results underscore the need for a material-specific framework to guide the rational design of hydrogels as antibacterial biomaterials, infection models, and platforms for studying microbe–material interactions.

Results

Low hydrogel concentrations promote increased bacterial growth

To investigate the effect of hydrogel concentration, we first studied bacterial growth separately in US and S agarose hydrogels. These hydrogels were prepared at concentrations of 0.2%, 0.5%, and 1%, each encapsulating a defined nutrient medium (NB, LB, TSB, M1, and M2). Bacterial cultures were inoculated at the centre of the gels and incubated at 37 °C for 18 h. Growth areas (Figs. S2–S9) were quantified using Fiji software (Fig. S1).

Our results demonstrated that the growth of uropathogenic *E. coli, P. fluorescens, S. aureus, and B. subtilis* increased progressively with decreasing hydrogel concentration (Fig. 2). Notably, reductions from 1% to 0.2% and from 0.5% to 0.2% led to 82.5% and 55% increase in bacterial growth, respectively, across both US and S hydrogels. Even a modest concentration decrease from 1% to 0.5% resulted in a 27.5% growth increase, indicating that bacterial growth is highly sensitive to small changes in hydrogel concentration. These findings demonstrate a strong positive effect of lower hydrogel concentrations on bacterial growth.

To explore structural differences underlying the observed growth patterns, we performed cryo-SEM imaging of US and S hydrogels at varying concentrations (Fig. S10). In US hydrogels, higher agarose concentrations (1%) showed smaller, denser pores, while lower concentrations (0.5%) exhibited visibly larger pores. S hydrogels displayed a distinct thread-like network, with 1% gels forming more compact structures than 0.5%. These morphological differences suggest that lower hydrogel concentrations

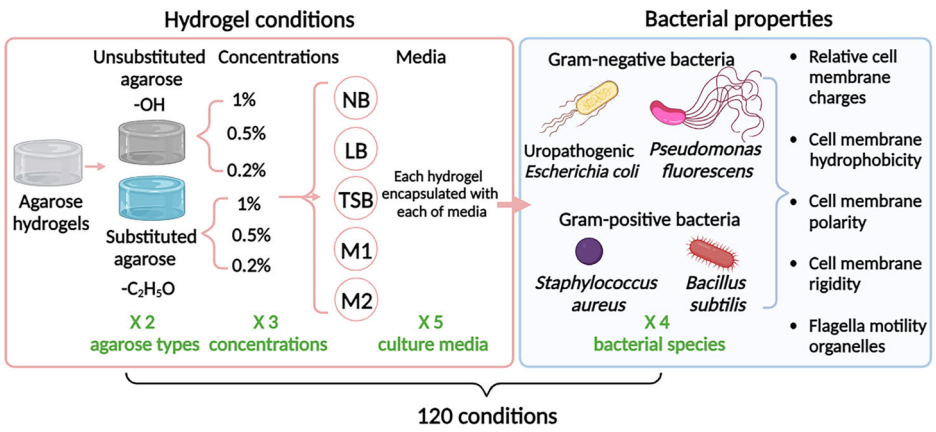

Fig. 1 | Schematic illustration of the multi-parametric study involving hydrogel conditions and bacterial properties. 2 types of agarose hydrogels namely, unsubstituted and substituted hydrogels, each at 3 different concentrations of 1%, 0.5%, and 0.2% encapsulated with 5 different nutrient media including NB, LB, TSB, M1, and M2 were included for assessment of bacterial growth. The growth of 4 different bacterial species including *E. coli* and *P. fluorescens* (Gram-negative), and *S. aureus* and *B. subtilis* (Gram-positive) bacterial species were studied. In total, the study included 120 conditions.

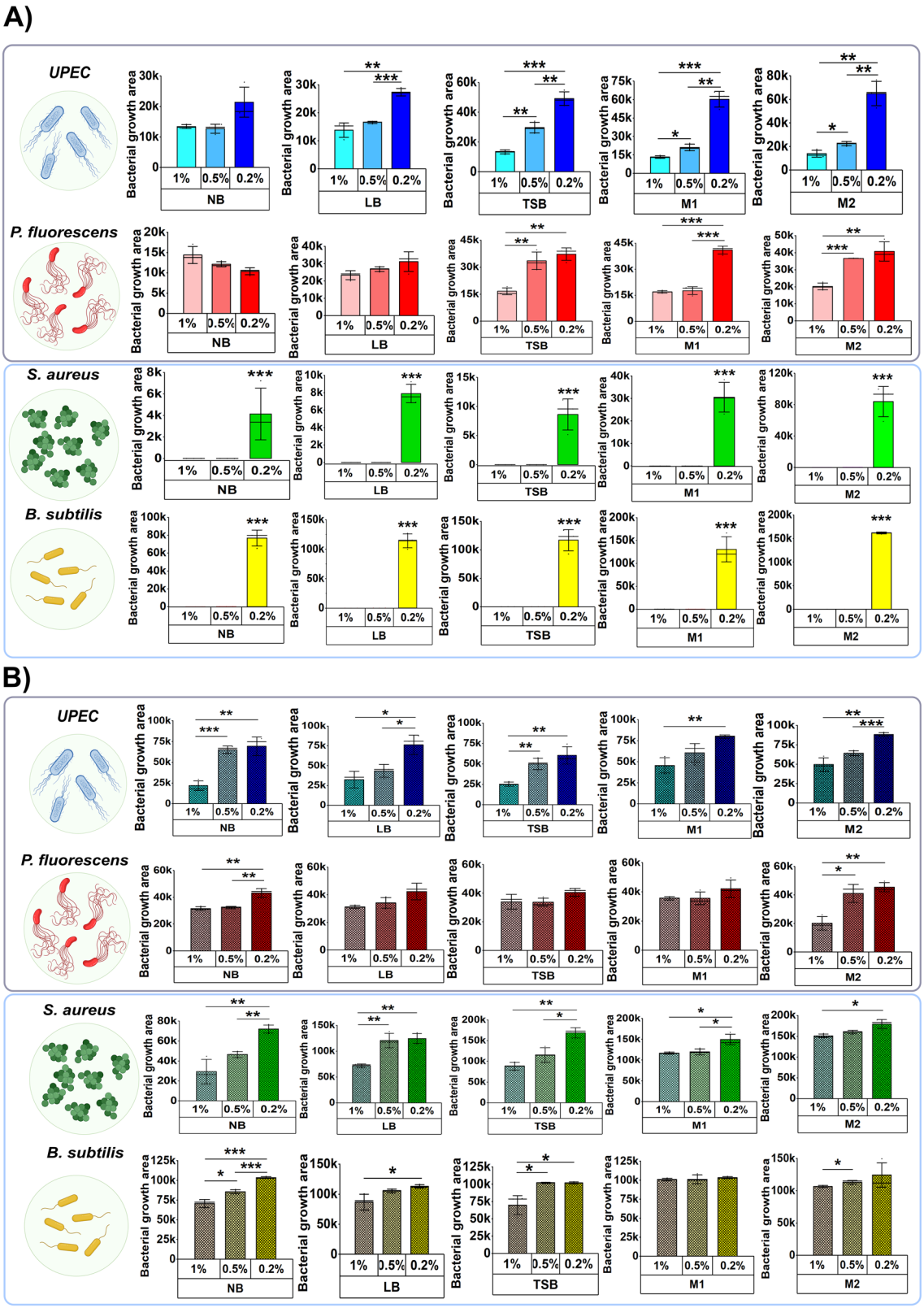

Fig. 2 | Quantitative evaluation of bacterial growth on agarose hydrogels. Growth of (i) uropathogenic *E. coli*, (ii) *P. fluorescens*, (iii) *S. aureus*, and (iv) *B. subtilis* in NB, LB, TSB, M1, and M2 – encapsulated unsubstituted (**A**) and substituted (**B**) agarose hydrogels, each at 1%, 0.5%, and 0.2% hydrogel concentrations. Data are presented as mean ± standard deviation (SD) from $n = 3$ independent replicates. Statistical significance was assessed using ANOVA. $^{*}P < 0.05$, $^{**}P < 0.01$, and $^{***}P < 0.001$.

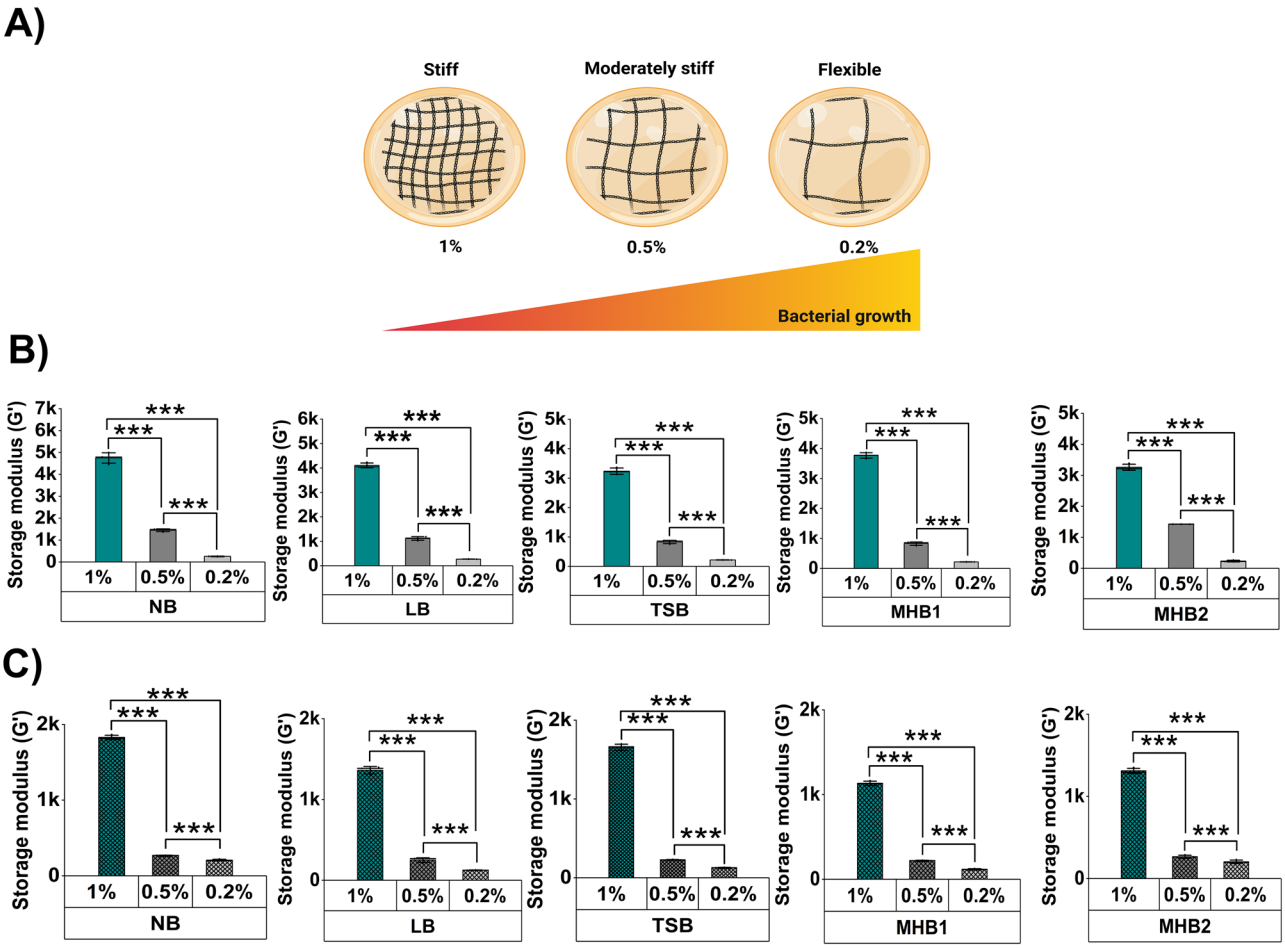

Fig. 3 | Effect of agarose concentration on stiffness of agarose hydrogels. **A** Schematic showing decreasing agarose concentrations (1% → 0.5% → 0.2%) with varying crosslinking and stiffness. Storage modulus (G') of **B** US and **C** S hydrogels with NB, LB, TSB, M1, and M2 at varying concentrations. Data are presented as mean ± standard deviation (SD) from $n = 3$ independent replicates. Statistical significance was assessed using ANOVA. P value: $^{*}P < 0.05$, $^{**}P < 0.01$, $^{***}P < 0.001$.

support greater porosity, potentially enhancing nutrient transport and facilitating bacterial proliferation.

To determine whether bacteria proliferate solely at the hydrogel surface or also within the bulk, we performed Z-stack imaging of GFP-tagged *E. coli* in 1% and 0.2% US hydrogels. Bacteria were observed throughout the hydrogel network in both concentrations, with deeper penetration and more uniform distribution in the softer 0.2% hydrogel (Figs. S11 and S12). These observations indicate that growth occurs both at the surface and within the hydrogel bulk, supporting the relevance of hydrogel physiochemical properties in controlling bacterial colonization throughout the 3D network.

Hydrogel stiffness scales with polymer concentration

To investigate the physical basis for the observed concentration-dependent increase in bacterial growth, we assessed how polymer concentration influences the mechanical properties of the hydrogels. Quantitative rheological measurements showed a marked decrease in storage modulus (G′) with decreasing agarose concentration, consistent across both US (Fig. 3B) and S (Fig. 3C) hydrogels. Specifically, stiffness decreased from 3825 ± 630 Pa (US) and 1479 ± 270 Pa (S) at 1%, to 1130 ± 300 Pa (US) and 245 ± 22 Pa (S) at 0.5%, and further to 240 ± 24 Pa (US) and 156 ± 46 Pa (S) at 0.2%. The amplitude and frequency sweep curves of hydrogels are provided in Figs. S13–S22. Reported storage moduli for substituted agarose in the literature are higher, ranging from ~6.6×10^3 Pa at 0.75% to 1.1×10^5 at 3% (Guégan et al.[26]), reflecting differences in polymer concentration, substitution chemistry, and the absence of varying nutrient media. The reduction in stiffness aligns with the increased bacterial growth observed at lower concentrations, suggesting that softer hydrogel networks provide a more permissive environment for proliferation.

Lower polymer content preserves hydrogel water retention

Alongside stiffness evaluation, we also determined the water retention capacity of our hydrogels. Studies have suggested that the water content of hydrogels may influence bacterial growth behaviour[28]; however, this aspect remains understudied. Indeed, the hydrophilicity of the hydrogel play a key role in regulating water retention, nutrient availability, and diffusion within the hydrogel network, thereby influencing bacterial colonization. Determination of water retention is even more important in cases where hydrogels are incubated at 37 °C for 18 h, as water evaporates quickly during this time, interfering with bacterial growth. To assess this effect, we measured the weights of hydrogels before and after incubation. Interestingly, we identified the highest and statistically significant water loss in the stiffest 1% hydrogels compared to intermediately stiff 0.5% and flexible 0.2% hydrogels, in both US (Fig. 4B) and S (Fig. 4C) hydrogels across all nutrient media encapsulated formulations.

Combined effects of stiffness and water loss on bacterial growth

To provide a broader overview of the influence of hydrogel stiffness and water loss on bacterial growth, we analysed and combined the data into heatmaps (Fig. S24). When considering US and S hydrogels separately, one observes increasing bacterial growth from 1% to 0.2% for both stiffness and water loss. When this data is combined into a single heatmap (with US on the left and S on the right), a non-linear pattern, as shown for *E.coli* in Fig. 5A, becomes evident, with all values seeming to increase from left to

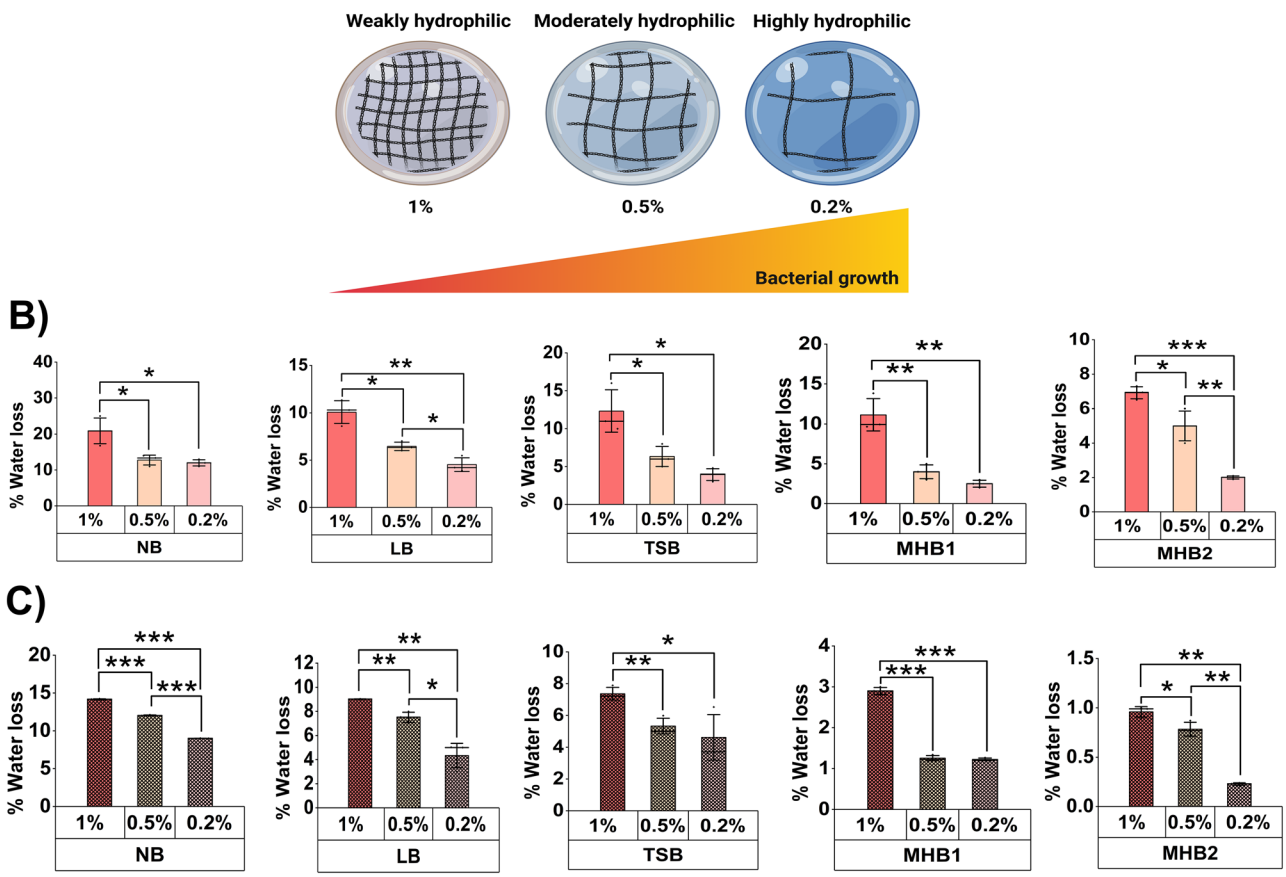

Fig. 4 | Effect of agarose concentration on water loss properties of agarose hydrogels. A Schematic showing decreasing agarose concentrations (1% → 0.5% → 0.2%) with varying crosslinking and hydrophilicity. % Water loss of **B** US and **C** S hydrogels with NB, LB, TSB, M1, and M2 at varying concentrations. Data are presented as mean ± standard deviation (SD) from $n = 3$ independent replicates. Statistical significance was assessed using ANOVA. P value: $^{*}P < 0.05$, $^{**}P < 0.01$, $^{***}P < 0.001$.

right, with the exception of the third column (US 0.2%) that consistently exhibits higher values (for stiffness, water loss and growth) than the fourth column (S 1%). This clear repeating pattern hints at a strong correlation between bacterial growth, stiffness and water loss, independent from the hydrogel type. This observation is confirmed in Fig. 5B that shows a consistent and progressive growth pattern obtained after rearranging the heatmaps in order of decreasing stiffness and water loss.

The above observation is not only limited to *E. coli* but is also observed in *P. fluorescens* growth (Fig. S23). In contrast, *S. aureus* and *B. subtilis* showed more complex trends, involving electrostatic interactions (described below). Indeed, 3D heatmaps in Fig. 5E–H show the growth of all bacterial species arranged as function of stiffness and water loss irrespective of the hydrogel type. Similar trends are observed for all bacterial species; a negative association between both stiffness and water loss was seen with bacterial growth, as confirmed using Spearman's correlation (Tables S25 and S26). The correlation coefficients indicate a strong inverse relationship for all species (P values ranging from −0.56 to −0.80), quantitatively supporting the mechanistic link between hydrogel stiffness, water retention, and bacterial growth. We also note species-specific responses. While *E. coli* followed the trend, *P. fluorescens* showed slightly higher growth in 1% S than 0.2% US in some media, though differences were statistically insignificant ($P > 0.05$, Fig. 5E, F). For *S. aureus* and *B. subtilis*, growth was inhibited in 1% and 0.5% US, but minimal growth was observed in 0.2% US (Fig. 5G, H). We also note that, S hydrogels enhance bacterial growth compared to US hydrogels due to their improved elasticity and water content. Importantly, these trends can be explained by higher crosslinking density of stiffer agarose networks, which reduces water-holding capacity and increases water loss. As a result, bacteria in stiffer, dehydrated hydrogels experience limited nutrient transport, greater mechanical confinement, and desiccation stress, whereas softer, more hydrated networks provide a more permissive environment for expansion and metabolic activity. Overall, these results demonstrate that lower hydrogel stiffness and reduced water loss promote bacterial growth, although the magnitude and nature of this effect remain species dependent.

The pronounced growth of Gram-positive bacteria (*S. aureus* and *B. subtilis*) in 0.2% US hydrogels reflects the interplay of hydrogel mechanics, hydration, and bacterial envelope properties. At this low polymer concentration, the network is softer and retains more water, reducing mechanical confinement and desiccation stress, which facilitates proliferation. The low crosslinking density also likely diminishes electrostatic inhibition, allowing Gram-positive bacteria with thick peptidoglycan walls to grow more effectively than in stiffer matrices. These results highlight that bacterial responses are species-specific and shaped by a combination of stiffness, hydration, and surface interactions, rather than bulk hydrogel properties alone.

Encapsulated nutrient media impacts bacterial growth by altering hydrogel stiffness and water loss

Further supporting our findings that bacterial growth correlates with decreasing hydrogel stiffness and water loss, we observed a surprising effect of encapsulated nutrient media on bacterial growth. Growth of *E. coli*, *P. fluorescens*, *S. aureus*, and *B. subtilis* was tested in NB, LB, TSB, M1, and M2,

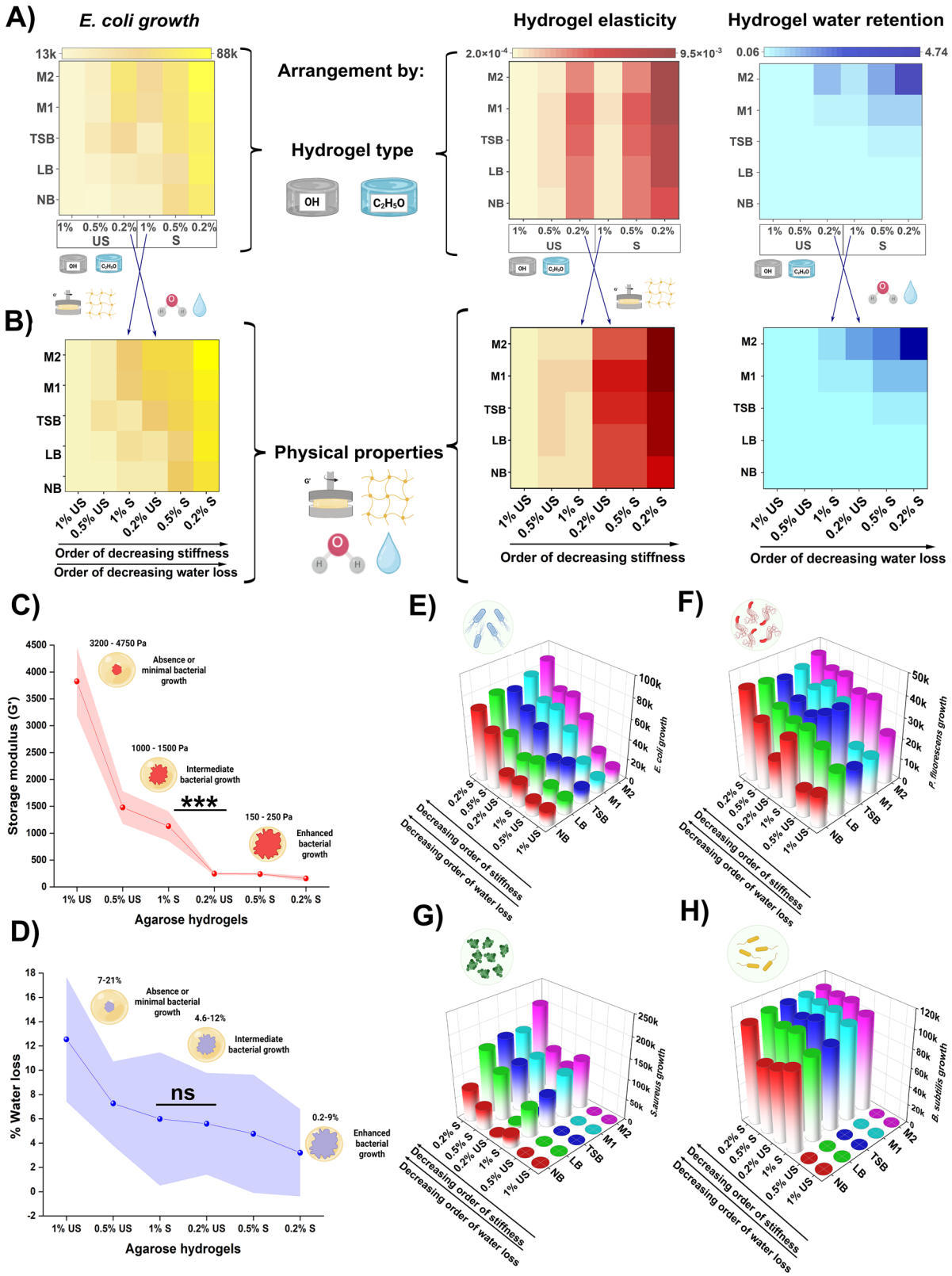

Fig. 5 | Relationship between hydrogel properties and bacterial growth patterns. Heatmaps indicating the growth of *E. coli* according to **A** hydrogel type, hydrogel elasticity and water retention and **B** in order of decreasing hydrogel stiffness and water loss. **C** Storage modulus (G') ($^{***}P < 0.001$) indicating increasing stiffness with US and S hydrogels combined: 0.2% S < 0.5% S < 0.2% US < 1% S < 0.5% US < 1% US. **D** % water in US and S hydrogels combined: 0.2% S < 0.5% S <(0.2% US = 1% S) < 0.5% US < 1% US. Maximum bacterial growth occurs in hydrogels with 150–250 Pa stiffness and 0.2–9% water loss. Growth of **E** *E. coli*, **F** *P. fluorescens*, **G** *S. aureus*, and **H** *B. subtilis* increases with decreasing hydrogel stiffness and water loss. US contains only -OH groups, whereas S hydrogels contain additional -C_2H_5O/-CH_2CH_2OH groups, which enhance hydrophilicity. The chemical structures are illustrated in Fig. S27.

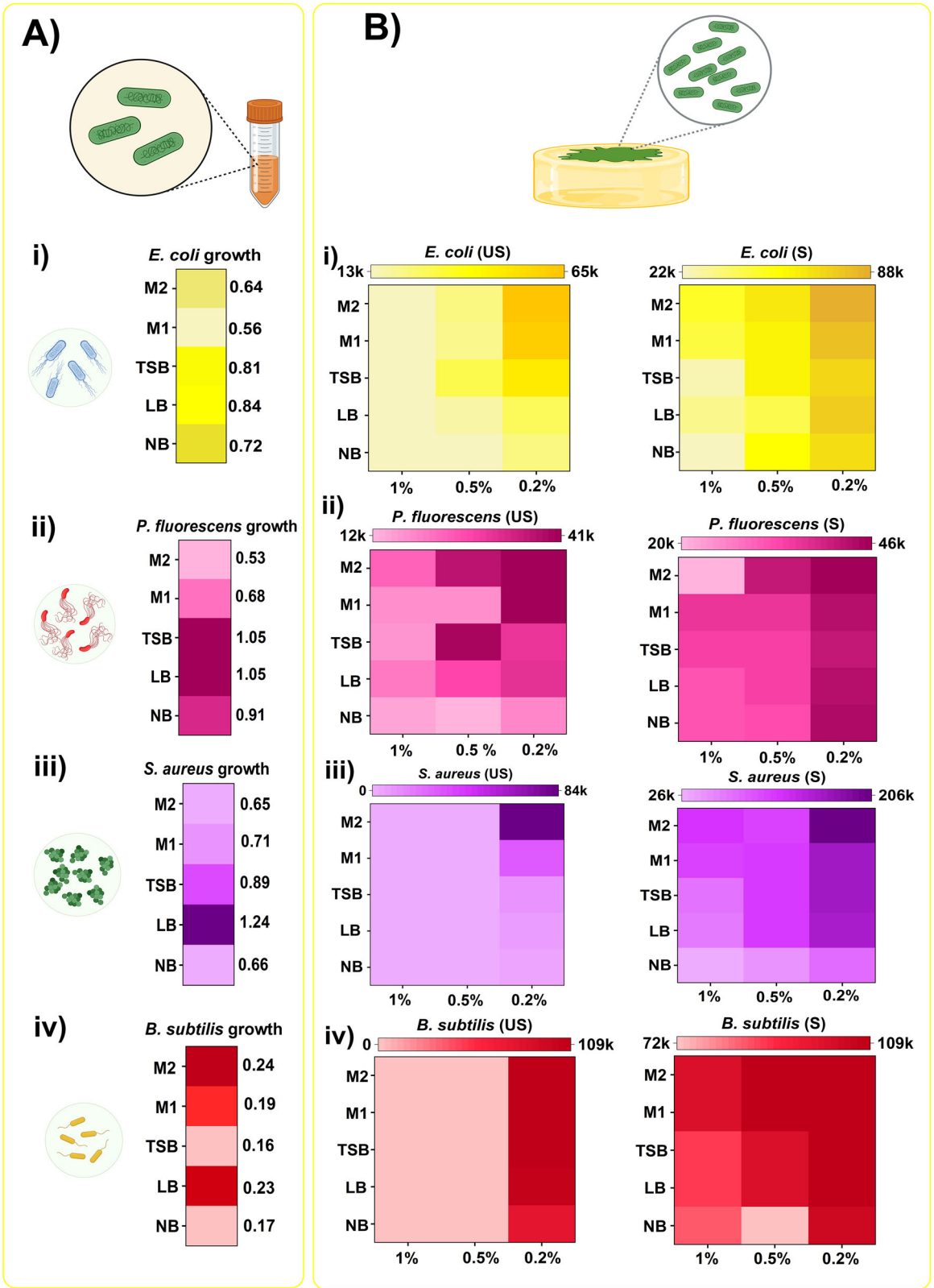

Fig. 6 | Effect of encapsulated nutrient media on bacterial growth. Heatmaps showing the effect of nutrients on (i) *E. coli*, (ii) *P. fluorescens*, (iii) *S. aureus*, and (iv) *B. subtilis* growth **A** in-solution show no consistent pattern, likely driven by media composition. **B** In hydrogels (1%, 0.5%, 0.2%) with encapsulated NB, LB, TSB, M1, and M2, growth is more consistent-highest in M2 across all species.

both in-solution and in hydrogels. In-solution growth varied across media and species without a clear pattern (Fig. 6A). When hydrogels (1%, 0.5%, and 0.2% US and S) were encapsulated with these media, 90% of the hydrogels showed significantly greater bacterial growth in M2 compared to NB. Heatmap analysis (Fig. 6B) revealed that M2 encapsulation led to increased bacterial growth, while NB consistently showed the lowest growth, suggesting media components interact with the hydrogel network to restrict bacterial growth. LB, TSB, and M1 hydrogels showed intermediate growth.

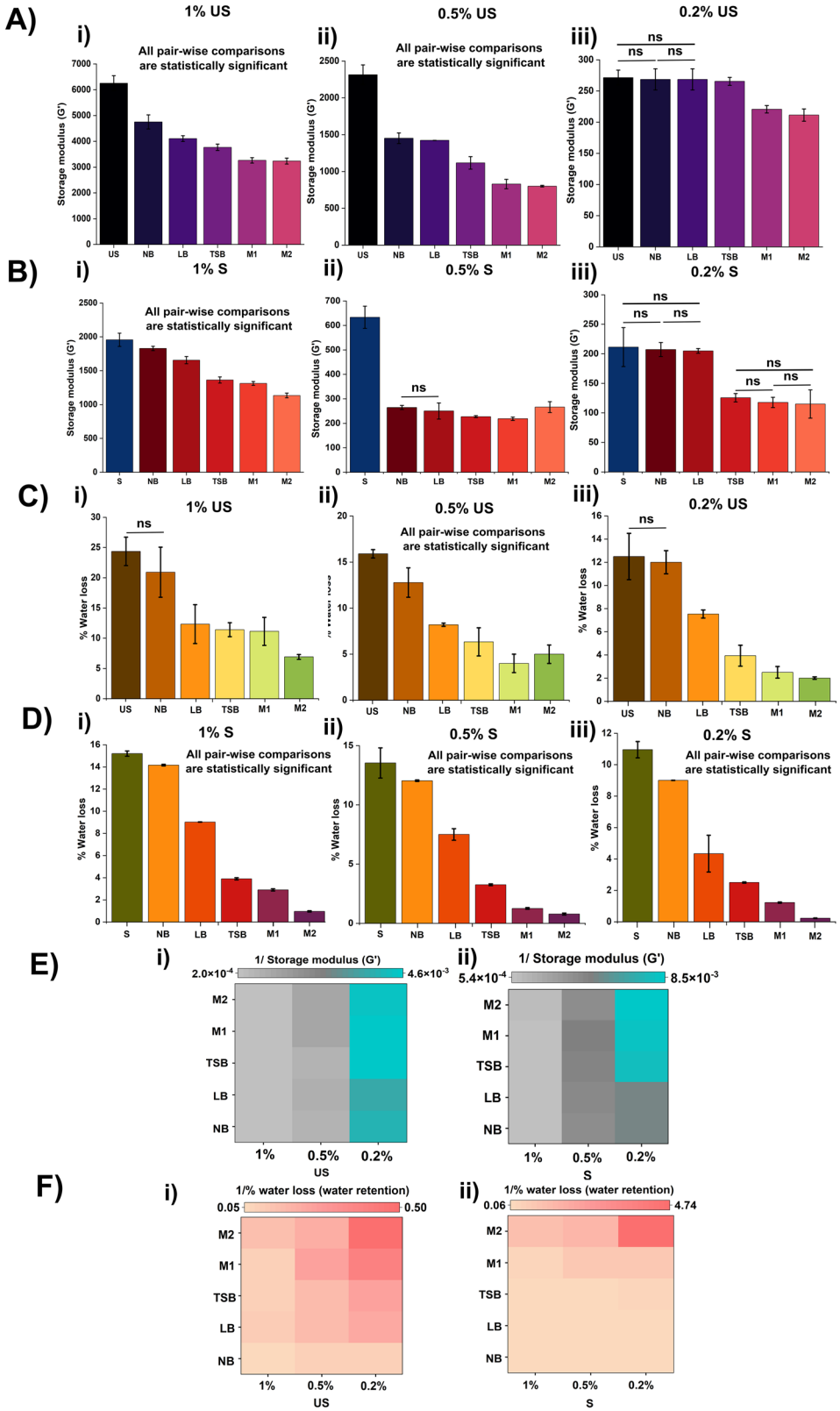

Fig. 7 | Nutrient-dependent changes in hydrogel mechanics and bacterial growth. Effect of nutrient on hydrogel properties and bacterial growth (**A**), **B** Stiffness of US (i) 1%, (ii) 0.5%, and (iii) 0.2% and 1%, (ii) 0.5%, and (iii) 0.2% S hydrogels encapsulated with NB, LB, TSB, M1, and M2. **C**, **D** % water loss of US (i) 1%, (ii) 0.5%, and (iii) 0.2% and 1%, (ii) 0.5%, and (iii) 0.2% S hydrogels encapsulated with NB, LB, TSB, M1, and M2. Data are presented as mean ± standard deviation (SD) from $n = 3$ independent replicates. ANOVA test was performed with statistical significance set to a $P < 0.05$. Non-significant comparisons are indicated as 'ns'. **E** Heatmap of elasticity (1/stiffness) and **F** water retention (1/water loss) shows M2-encapsulated hydrogels have highest elasticity and water retention.

To investigate this interaction, we examined the stiffness and water loss properties of US and S agarose hydrogels encapsulated with NB, LB, TSB, M1, and M2. Compared to NB, all other media (LB, TSB, M1, and M2) resulted in a noticeable reduction in hydrogel stiffness across all concentrations (1%, 0.5%, 0.2%) with M2 producing the greatest decrease in US (Fig. 7A(i–iii)) and S (Fig. 7B(i–iii)). Similarly, water retention was higher (i.e. lower water loss) in hydrogels containing LB, TSB, M1, and M2, relative to NB in US (Fig. 7C(i–iii)) and S (Fig. 7D(i–iii)).

Our findings indicate that encapsulated nutrients influence hydrogel stiffness and water loss, thereby affecting bacterial growth. To illustrate this, we plotted inverted stiffness (Fig. 7E(i, ii)) and water loss values (Fig. 7F(iii, iv)) as proxies for elasticity and water retention, respectively. These heatmaps reveal that media such as TSB, M1, and M2 produce more elastic and

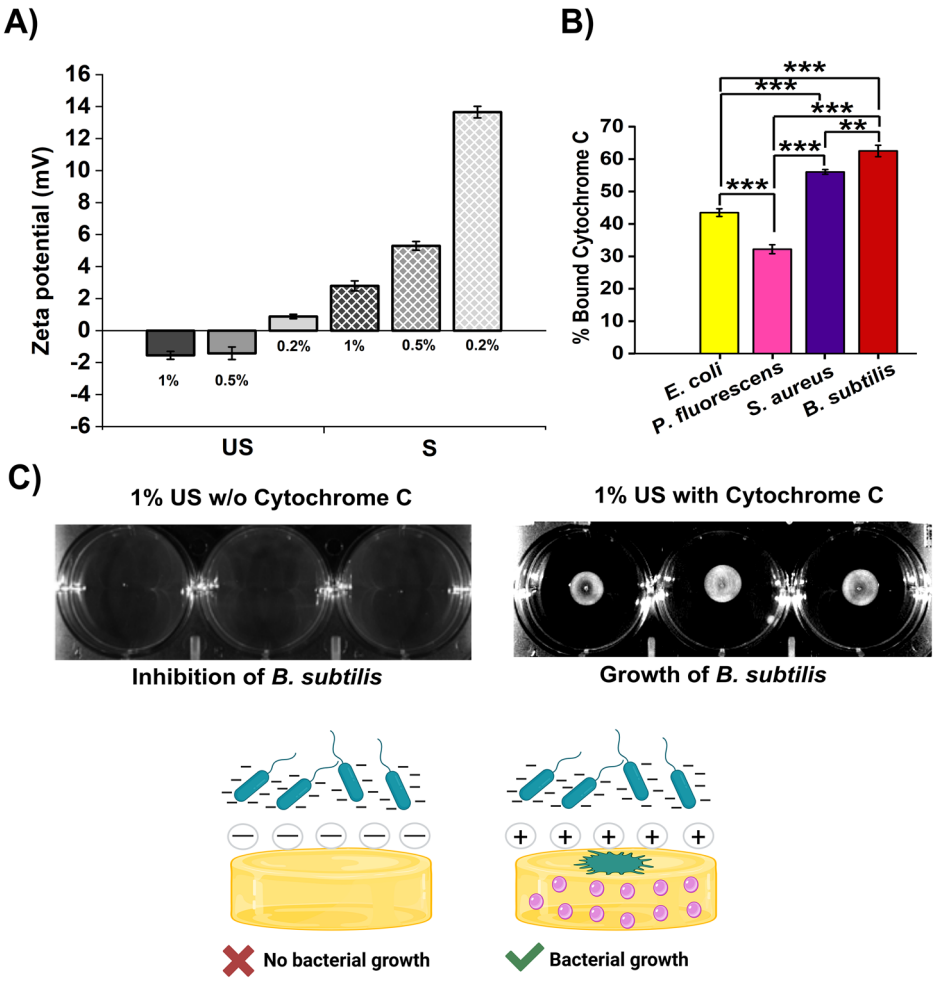

Fig. 8 | Evaluation of electrostatic interactions between bacteria and hydrogels. A Zeta potentials of US and S hydrogels (1%, 0.5%, and 0.2%) show surface charge differences. **B** Cytochrome C assay reveals bacterial binding affinities. Data are presented as mean ± standard deviation (SD) from $n = 3$ independent replicates. Statistical significance was assessed using ANOVA. P value: $^{*}P < 0.05$, $^{**}P < 0.01$, $^{***}P < 0.001$. **C** *B. subtilis* growth inhibition on negatively charged 1% US hydrogels. Growth restored in 1% US hydrogel encapsulated with cytochrome C (in pink).

water-retaining hydrogels. These trends align with conditions that support greater bacterial growth, suggesting that increased hydrogel elasticity and water retention promote bacterial proliferation. While these media were observed to soften hydrogels and improve water retention, the precise physiochemical mechanisms such as ionic strength effects or protein polysaccharide interactions were not investigated here and remain a topic of future study.

Furthermore, we assessed the hydrophilicity of US and S agarose hydrogels. Contact angle measurements revealed that substituted hydrogels (1%, 0.5%, 0.2%) exhibit moderate wettability, with contact angles of 76.6°, 62.1°, and 58.5°, respectively (Supplementary Fig. S28), indicating that substitution with hydroxyethyl groups increases hydrophobicity. When encapsulated with bacterial nutrient media, these hydrogels became more hydrophilic (Supplementary Movies 1–5), suggesting that media components can modify hydrogel properties. In contrast, unsubstituted hydrogels were inherently hydrophilic, and encapsulating media did not affect their hydrophilicity (Supplementary Movies 6–10). These findings demonstrate that encapsulated nutrient media alter hydrogel stiffness, water retention, and surface wettability, thereby influencing bacterial growth.

Unsubstituted agarose hydrogels selectively promote/inhibit bacterial growth

Interestingly, growth assays revealed that 0.5% and 1% US hydrogels promoted *E. coli* and *P. fluorescens* growth, but inhibited *S. aureus* and *B. subtilis*, while 0.2% hydrogels supported minimal growth (Figs. 2, 5G, H, S27 and S28). To understand this selective inhibition, we investigated bacterial cell surface properties, particularly the surface charge, and how this impacts interaction with the hydrogel matrix.

Zeta potential measurements showed that 0.5% and 1% US hydrogels are negatively charged (-1.42 ± 0.39 and -1.54 ± 0.25), while 0.2% unsubstituted and all substituted hydrogels are positively charged (Fig. 8A). Zeta potential measurements on bacteria revealed that Gram-negative (*E. coli*, *P. fluorescens*) exhibit more negative overall charges (–37 mV and –33 mV) compared to Gram-positive bacteria (*S. aureus*, *B. subtilis*, –18 mV and –25 mV). Cytochrome C, a small positively charged heme protein commonly used to assess surface charge; its binding to bacterial cells serves as an indicator of cell surface negativity. Cytochrome C binding assays probe exposed surface charges, showed that *S. aureus* and *B. subtilis* possess highly negative surface charges (56% and 62.5%), whereas *E. coli* and *P. fluorescens* are less negative (43% and 32%) (Fig. 8B). These results indicate that although Gram-negative bacteria are more negative overall, their exposed negative charges are shielded by the outer membrane, whereas Gram-positive bacteria have exposed negatively charged teichoic acids that interact strongly with negatively charged US hydrogels. Consequently, electrostatic repulsion inhibits Gram-positive growth. To test this mechanism, positively charged cytochrome C was embedded into 1% US hydrogels, which reversed the inhibitory effect and restored B. subtilis growth (Fig. 8C), confirming that exposed surface charges play a key role in bacterial compatibility with hydrogels.

To evaluate whether other factors such as differences in cell wall structure, biofilm initiation capacity, or surface hydrophobicity could also influence bacterial interactions with hydrogels, we assessed the potential role of bacterial cell surface properties. We measured hydrophobicity, membrane rigidity, and polarization (Fig. S30). Although minor differences were observed between species, none showed a consistent correlation with the differential growth patterns, further supporting that electrostatic

interactions are the dominant factor governing selective bacterial growth on agarose hydrogels.

Discussion

Our study demonstrates that the physicochemical properties of agarose hydrogels play a significant role in regulating bacterial growth. By systematically varying the hydrogel type, hydrogel concentration, and the composition of the encapsulated nutrient media, we show that bacterial growth is influenced not only by nutrient availability but also by the mechanical stiffness, hydration capacity, and electrostatic characteristics of the hydrogel. Some species in our study are flagellated (*E. coli, P. fluorescens, B. subtilis*) while *S. aureus* is non-flagellated. Although motility phenotypes were confirmed in standard soft-agar assays, active motility was not tested directly in hydrogels. Nonetheless, observed growth patterns across species suggest that hydrogel physicochemical properties, rather than motility, are the primary determinants of proliferation. Together, these findings indicate that the physical and chemical properties of the hydrogel matrix are dominant regulators of bacterial growth, highlighting the importance of considering matrix stiffness, hydration, and electrostatic interactions when designing hydrogel-based bacterial models or antimicrobial materials.

We show that hydrogel stiffness and water content are critical determinants of bacterial growth, with softer and more hydrated networks consistently supporting greater growth across all tested bacterial species. In our experimental setup, bacterial inoculation was performed by pricking the hydrogel surface, thereby providing entry points through which bacteria could infiltrate the matrix and establish growth both at the surface and within the hydrogel interior. This configuration bridges surface-associated and partially invasive environments and may better reflect natural settings where bacteria interact dynamically with soft materials[16,25,33]. The enhanced growth in softer hydrogels suggests that reduced mechanical resistance facilitates both nutrient transport and spatial expansion, while higher water retention maintains a stable microenvironment that protects against desiccation. Interestingly, in the softer 0.2% hydrogels especially US ones, *E. coli* exhibited elongated morphologies, where bacteria in 1% gels remained normal rod-shaped (Figs. S11 and 12). This elongation may reflect enhanced motility or swarming-like behaviour facilitated by the softer, mechanically permissive environment, highlighting that hydrogel stiffness can modulate not only bacterial proliferation but also phenotypes and behaviour. Further studies are needed to fully understand the mechanisms underlying morphological changes and its implications in bacterial colonization.

Notably, previous studies have reported inconsistent relationship between hydrogel stiffness and bacterial growth, likely due to differences in bacterial localisation (surface vs. bulk matrix), unaccounted water loss characteristics, or varying definitions of mechanical compliance[26,28,31]. Together, our findings provide a mechanistic explanation for how hydrogel properties modulate bacterial growth.

Varying hydrogel polymer concentration modulates bacterial growth. Higher concentrations produce stiffer, less hydrated networks that restrict expansion and nutrient transport, while lower concentrations create softer, hydrated matrices that promote proliferation. Heatmaps (Figs. 5, S23 and S24) show growth increasing from 1% to 0.2% for most species, with Gram-positive bacteria also affected by electrostatic interactions in unsubstituted hydrogels. These results demonstrate that polymer concentration controls growth through mechanical, hydration, and species-specific factors. To rigorously validate these findings, we performed a Type-I four-way factorial analysis of variance (ANOVA) with bacterial species, hydrogel type, polymer concentration, and encapsulated nutrient medium as independent variables (Table S29). While mechanical stiffness and water retention were not included explicitly as independent factors, these physical properties are emergent from the combination of the tested variables. The statistical analysis revealed that all main effects and interaction terms were highly significant (Table S29), with the most pronounced effects arising from the species–hydrogel type interaction ($F = 617.53$) and a strong three-way interaction involving hydrogel concentration ($F = 123.31$). These results underscore the multifactorial nature of bacterial growth regulation and the importance of species-specific responses to the mechanical and hydration properties of the hydrogel matrix.

In addition to mechanical and hydration effects, our findings reveal the active and dual role of the encapsulated nutrient media, not only as a metabolic substrate for bacterial growth but also as a modulator of hydrogel physicochemical characteristics. While previous studies have shown that nutrient components like tryptone can modulate hydrogel stiffness by interacting with polymer network[25], our work extends this understanding by demonstrating that media composition also governs the hydrogel's water retention capacity, a factor not explicitly addressed by earlier reports. By showing that media composition influences both hydrogel stiffness and water content, we reveal how these physicochemical changes indirectly dictate bacterial proliferation. These results highlight the importance of considering medium-matrix interactions as integral to experimental design, particularly in hydrogel-based infection or colonization models.

Our results reveal species-specific responses to hydrogel properties. Gram-negative bacteria (*E. coli*, *P. fluorescens*) grew best in softer, hydrated hydrogels, with *E. coli* showing elongation in the softest gels. Gram-positive bacteria (*S. aureus*, *B. subtilis*) were more sensitive to polymer concentration, with growth restricted in stiffer, dehydrated matrices. These findings indicate that while stiffness and hydration broadly influence growth, species-specific traits produce important exceptions, emphasizing the need to consider both bacterial and matrix properties. Notably, we identify electrostatic interactions as a species-selective regulatory mechanism. Growth inhibition of Gram-positive bacteria in negatively charged unsubstituted agarose is attributable to surface charge repulsion, which was reversed by modifying the hydrogel charge via cytochrome C encapsulation. This observation highlights an underexplored dimension of hydrogel-bacteria interactions, in which physicochemical mismatch between hydrogel charge and bacterial envelope can serve as a selective growth-modulating mechanism.

Collectively, our results establish a comprehensive framework for understanding how the mechanical, hydration, and electrostatic properties of agarose hydrogels regulate bacterial growth. These findings have broad implications for the rational design of smart biomaterials that either promote or inhibit bacterial colonization. Such insights are directly relevant to the development of more physiologically relevant in vitro infection models, antimicrobial coatings, and biosensing platforms. Importantly, our study highlights the necessity of integrating material properties with microbiological design to harness the full potential of hydrogel-based technologies.

Our findings have direct implications for understanding bacterial behaviour in infection-relevant environments. Soft, hydrated matrices such as those found in wound beds, damaged tissue, or biomaterial coatings may promote bacterial proliferation by reducing mechanical resistance preventing desiccation. Conversely, stiffer or dehydrated matrices may hinder bacterial expansion and nutrient access, helping to restrict colonization. Furthermore, the observed role of matrix charge in selectively inhibiting certain species suggests a material-dependent mechanism that could be exploited to prevent surface colonization on medical devices or wound dressings. Since bacterial persistence and antibiotic tolerance are strongly influenced by local microenvironments, these results provide a mechanistic foundation for designing more realistic in vitro infection models and for engineering materials that either prevent or sustain bacterial colonization in a controlled manner.

Materials and methods

Bacterial culture

P. fluorescens and *S. aureus USA 300 JE2* (BEI Resources) was obtained from Warwick Medical School, and *B. subtilis 168* was obtained from Nanosyrinx, University of Warwick. The strain of *E. coli* used was Uropathogenic *E. coli* CFT073. Bacteria were revived from their glycerol stocks and streaked on lysogeny agar for *E. coli*, *P. fluorescens*, and *B. subtilis* and tryptic soy agar for *S. aureus*. Single colonies were picked from each plate and inoculated into the Luria broth medium for *E. coli*, *P. fluorescens*, and *B. subtilis* and TSB for

S. aureus for primary culture at 37 °C and 180 RPM overnight. The optical density (OD) of bacterial cultures was determined at 600 nm. The bacterial cultures were adjusted to an OD of 0.1 using culture medium appropriate for each bacterial species. 2 µL of these cultures were utilised for evaluating bacterial growth in agarose hydrogels.

Bacterial growth experiments were performed at 37 °C to provide a consistent, physiologically relevant temperature for infection-related conditions. While *E. coli* and *S. aureus* are naturally adapted to this temperature, *P. fluorescens* and *B. subtilis* may have slightly lower optimal growth temperatures. Pilot experiments confirmed that all species grew robustly at 37 °C, allowing direct comparisons across hydrogel types and concentrations without introducing temperature-dependent variability.

Synthesis of bacterial culture media encapsulated agarose hydrogels

Unsubstituted agarose hydrogels were prepared using high-melting agarose of molecular grade (BIO-41025, lot number: ES520-B103080) purchased from Meridian Biosciences, Bioline. High-melting agarose has a melting temperature of 88.8 °C and gelling temperature of 38.5 °C. Substituted agarose hydrogels were prepared using low-melting agarose of hydroxyethyl type (product number: A9414, CAS number: 39346-81-1) purchased from Sigma-Aldrich, Merck. Low-melting agarose has a melting temperature of ~65 °C and gelling temperature of 26−30 °C.

Agarose hydrogels were prepared in batches of 50 mL for each type of nutrient media and concentrations: 0.5 g agarose in 50 mL (1%), 0.25 g agarose in 50 mL (0.5%), 0.1 g in 50 mL (0.2%) for NB, LB, TSB, M1, and M2 media. The solutions were heated up to 100 °C until all the agarose was completely dissolved (~ <2 min). 2 mL of these agarose solutions were pipetted onto sterile tissue culture graded 6-well plates (Greiner) and allowed to gel at room temperature, yielding ~2.1 mm thick hydrogels. For each of these conditions, the experiments were performed in three replicates. To ensure complete hydrogel solidification, the plates were used for experiments after 45 min of gelation.

Bacterial growth in hydrogels

Once the hydrogels were solidified, 2 µL of bacterial cultures were introduced separately for each condition. The bacterial culture was pricked at the centre of the agarose hydrogel in 6-well plate such that the prick penetrates the gel but does not pierce the hydrogel bottom. Upon bacterial introduction on hydrogels, the plates were incubated without any disturbance of physical movements at 37 °C for 18 h. Bacterial growth was qualitatively visualised using the BIO-RAD ChemiDoc™ MP imaging system using the colorimetric filter with an exposure time of 50 s. For *B. subtilis*, the exposure time was prolonged to 1.50 min due to their growth characteristics, which was not apparent in 50 s.

Fiji analysis

The colorimetric images were analysed in the Fiji software. All images were converted to 8-bit and a background subtraction was performed. The images were then adjusted by thresholding to focus on bacterial growth and rule out non-bacterial growth spots. After thresholding, the images were converted to the binary format for ease of segmentation and quantitative measurements of bacterial growth areas. The bacterial growth area was quantified using the measure function in Fiji, representing the two-dimensional area of bacterial spread.

Bacterial distribution imaging (Z-stack)

To assess bacterial distribution within hydrogels, we used *E. coli* S17.1 (pUB7 λpir with pBAM7 plasmid expressing green fluorescent protein (GFP). Bacteria were introduced in 1% and 0.2% US hydrogels as described above. For fluorescence microscopy (Leica DMi8 widefield microscope) hydrogels were prepared at ~500 µm total thickness by adding 50 µL of agarose per 1 cm^2 well in 4-well tissue culture-grade chamber slides. Although the gel thickness was 500 µm, the fluorescence microscope could capture only the optically accessible top ~12–14 µm of the hydrogel for Z-stack imaging with 100X oil immersion. Z-stacks images were acquired at 0.3 µm steps along the *Z*-axis, and maximum intensity projections were generated to visualise bacterial distribution within this region. Images were processed in ImageJ, converted to 8-bit with consistent brightness and contrast, thresholded to indicate bacteria, and analysed using the 3D Objects Counter Plugin to determine bacterial distribution along *X*, *Y*, and *Z* axes. A Z-histogram showing bacterial distribution with depth (µm) was also generated (Figs. S11 and S12).

Hydrogel stiffness – rheology

The stiffness of unsubstituted and substituted agarose hydrogels was determined by oscillatory rheology at 25 °C by monitoring the storage modulus (Young's modulus) (G') and loss modulus (G") using the parallel plate geometry in the Anton Paar MCR 302 rheometer. First, amplitude sweeps were performed at a constant frequency of $\omega = 10$ rad/s to determine the linear viscoelastic regions (LVE) for each concentration and hydrogel type. Frequency sweep analysis was performed in the angular frequency range of $\omega = 1–100$ rad/s with a constant strain of $\gamma = 0.05\%$ as determined from the amplitude sweep analysis using RheoCompass software.

Hydrogel hydrophilicity - contact angle measurements

The hydrophilicity of hydrogels was determined by contact angle measurements using the KRÜSS drop shape analyser 100. 5 µL of water was used for the measurements. KRÜSS DSA3 software with Young–Laplace mathematical model was used for recording the contact angle measurements.

Qualitative assessment of hydrogel porosity - Cryo-SEM

Cryo-SEM was performed using a Zeiss Crossbeam 550 (Carl Zeiss, Oberkochen, Germany) Focused Ion Beam Scanning Electron Microscope (FIB-SEM) at an accelerating voltage of 2 kV. The samples were maintained at cryogenic temperatures of −150 °C using a Quorum 3010 cryo stage (Quorum technologies, Loughton, UK). The samples were secured into slots in aluminium stubs mounted into the cryo-shuttle and plunged into slushy nitrogen and allowed to freeze. The cryo-sludge with samples was transferred to the preparation chamber and the samples freeze-fractured by a cooled blade. The fractured surface was sublimed at −90 °C for 30 min (etching). The temperature of the shuttle was returned to −150 °C and the samples were sputter coated with platinum at 10 mA for 60 s. Samples were transferred to the main stage of the microscope and imaged using a range of detection modes including the Secondary Electrons Secondary Ions and in-Lens detectors at 2 kV accelerating voltage. Standard imaging magnifications were used to allow comparison of different samples.

Water loss analysis

After hydrogel synthesis as described in 3.3.2, the 6-well plates were incubated at 37 °C for 18 h, mimicking the experimental conditions of bacterial growth on hydrogels. The weight of hydrogels before and after incubation for 18 h were recorded. The % water loss was calculated by:

$$\%\ water\ loss = hydrogel\frac{dry\ weight - wet\ weight}{dry\ weight} \times 100$$

Heatmaps and statistical analysis

All bar graphs and heatmaps were produced in OriginPro 2021b software.

A Type-I four-way factorial ANOVA was used to evaluate the effects of bacterial species, hydrogel type, polymer concentration, and encapsulated nutrient medium on bacterial growth. All main effects and interaction terms were included in the model. While hydrogel stiffness and water retention were not explicitly modelled as independent variables, they were treated as emergent properties resulting from the experimental design. ANOVA was performed using custom scripts written in R statistical programming language, which are publicly available at https://github.com/dtaylor3509/BacterialGrowthInHydrogels/tree/main.

The relationship between bacterial growth and hydrogel properties (stiffness and water loss) was assessed using Spearman's rank correlation. The storage modulus and % water loss measured values were used for correlation with bacterial growth.

Hydrogel charges - zeta potential analysis

The hydrogel surface charges were determined by measuring and analysing the zeta potential of hydrogels using the Anton Paar SurPASS 3 electrokinetic analyser. Discs with 1 cm diameter were punched out of agarose hydrogels and mounted into the recess of the cylindrical cell of the SurPass 3 instrument. The hydrogel discs were perforated with a tweezer to enable a continuous and laminar flow through the hydrogel. The discs were first put through five rinse cycles of 100 mL each at pressure of 600–200 mbar at a permeability index of 100–110 before zeta potential analysis. The zeta potential measurements were then determined at 25 °C with 10 mM potassium chloride in water and 10 mM PBS.

Overall bacterial charges – zeta potential analysis

The charges of bacterial cells were characterised by measuring the zeta potential of *E. coli*, *P. fluorescens*, *S. aureus*, and *B. subtilis* suspensions. Measurements were conducted using a Litesizer 500 (Anton Paar). Bacterial cells were harvested by centrifugation and washed three times with 10 mM HEPES buffer (pH = 7.4) to remove residual growth media components. The final cell suspensions were adjusted to an $OD_{600} = 0.1$. Zeta potential was determined based on electrophoretic mobility using the Smoluchowski approximation, with a Henry function (f(Ka)) of 1.5. Each reported value represents the mean of three independent measurements for each bacterial species. All measurements were performed at 25 °C.

Bacterial cell surface charges - cytochrome C assay

Primary cultures of *E. coli*, *P. fluorescens*, *S. aureus*, and *B. subtilis* were prepared as described above. The cultures were pelleted at 8000 RPM for 5 min and the pellet was washed with 20 mM (3-(N-morpholino) propanesulfonic acid) (MOPS) buffer, pH = 7. The cells were subsequently resuspended in MOPS buffer at an $OD_{600nm} = 1$. 50 μg/mL cytochrome C was added to the solution and incubated for 15 min at room temperature. The cells were pelleted at 8000 RPM for 5 min and the supernatant was used for spectrophotometric detection at OD_{410} using the FLUOstar OMEGA plate reader (BMG Labtech, UK) for measuring the unbound cytochrome C.

Data availability

The datasets used in the study are available in Figshare (DOI: 10.6084/m9.figshare.30531014).

Code availability

The R scripts used in this work are in Zenodo (https://doi.org/10.5281/zenodo.17524078) and GitHub (https://github.com/dtaylor3509/BacterialGrowthInHydrogels/tree/main).

Received: 22 July 2025; Accepted: 31 December 2025;
Published online: 22 January 2026

References

1. Fazeli-Nasab, B. et al. Biofilm production: a strategic mechanism for survival of microbes under stress conditions. *Biocatal. Agric. Biotechnol.* **42**, 102337 (2022).
2. Donlan, R. M. & William, C. J. Biofilms: survival mechanisms of clinically relevant microorganisms. *Clin. Microbiol. Rev.* **15**, 167–193 (2002).
3. Aertsen, A. & Michiels, C. W. Stress and how bacteria cope with death and survival. *Crit. Rev. Microbiol.* **30**, 263–273 (2004).
4. Kussell, E., Kishony, R., Balaban, N. Q. & Leibler, S. Bacterial persistence: a model of survival in changing environments. *Genetics* **169**, 1807–1814 (2005).
5. Emamalipour, M. et al. Horizontal gene transfer: from evolutionary flexibility to disease progression. *Front. Cell Dev. Biol.* **8** (2020).
6. Culyba, M. J. & van Tyne, D. Bacterial evolution during human infection: adapt and live or adapt and die. *PLoS Pathogens* **17**, https://doi.org/10.1371/journal.ppat.1009872 (2021).
7. Abbas, A., Barkhouse, A., Hackenberger, D. & Wright, G. D. Antibiotic resistance: A key microbial survival mechanism that threatens public health. *Cell Host Microbe* **32**, 837–851 (2024).
8. Huemer, M., Mairpady Shambat, S., Brugger, S. D. & Zinkernagel, A. S. Antibiotic resistance and persistence—Implications for human health and treatment perspectives. *EMBO Rep.* **21**, e51034 (2020).
9. Naghavi, M. et al. Global burden of bacterial antimicrobial resistance 1990–2021: a systematic analysis with forecasts to 2050. *Lancet* **404**, 1199–1226 (2024).
10. Keenan, K., Silva Corrêa, J., Sringernyuang, L., Nayiga, S. & Chandler, C. I. R. The social burden of antimicrobial resistance: what is it, how can we measure it, and why does it matter?. *JAC Antimicrob. Resist.* **7**, dlae208 (2025).
11. Poudel, A. N. et al. The economic burden of antibiotic resistance: a systematic review and meta-analysis. *PLoS ONE* **18**, e0285170 (2023).
12. Ahmad, M. & Khan, A. U. Global economic impact of antibiotic resistance: a review. *J. Glob. Antimicrob. Resist.* **19**, 313–316 (2019).
13. Bhattacharya, R., Bose, D., Gulia, K. & Jaiswal, A. Impact of antimicrobial resistance on sustainable development goals and the integrated strategies for meeting environmental and socio-economic targets. *Environ. Prog. Sustain Energy* **43**, e14320 (2024).
14. World Health Organization, Food and Agriculture Organization of the United Nations, United Nations Environment Programme & World Organisation for Animal Health. *A One Health Priority Research Agenda for Antimicrobial Resistance.* (World Health Organization, Geneva, 2023).
15. World Health Organization. Global research agenda for antimicrobial resistance in human health. (World Health Organization, Geneva, 2024). https://iris.who.int/handle/10665/379825.
16. Dsouza, A. et al. Multifunctional composite hydrogels for bacterial capture, growth/elimination, and sensing applications. *ACS Appl. Mater. Interfaces* **14**, 47323–47344. https://doi.org/10.1021/acsami.2c08582 (2022).
17. Yang, K. et al. Antimicrobial hydrogels: promising materials for medical application. *Int. J. Nanomed*. **13**, 2217–2263 (2018).
18. Chen, Q. et al. Intelligent design and medical applications of antimicrobial hydrogels. *Colloid Interface Sci. Commun.* **53**, 100696 (2023).
19. Hao, Z., Li, X., Zhang, R. & Zhang, L. Stimuli-responsive hydrogels for antibacterial applications. *Adv. Health. Mater.* **13**, 2400513 (2024).
20. Techakasikornpanich, M., Jangpatarapongsa, K., Polpanich, D. & Elaissari, A. Impact of polymeric films and hydrogels: physical characteristics on bacterial growth. *Polym. Adv. Technol.* **35**, e6311 (2024).
21. Sun, X., Ding, C., Qin, M. & Li, J. Hydrogel-based biosensors for bacterial infections. *Small* **20**, 2306960 (2024).
22. Yanez, F., Gomez-Amoza, J. L., Magarinos, B., Concheiro, A. & Alvarez-Lorenzo, C. Hydrogels porosity and bacteria penetration: where is the pore size threshold? *J. Memb. Sci.* **365**, 248–255 (2010).
23. Tuson, H. H. et al. Measuring the stiffness of bacterial cells from growth rates in hydrogels of tunable elasticity. *Mol. Microbiol.* **84**, 874–891 (2012).
24. Kolewe, K. W., Zhu, J., Mako, N. R., Nonnenmann, S. S. & Schiffman, J. D. Bacterial adhesion is affected by the thickness and stiffness of poly (ethylene glycol) hydrogels. *ACS Appl Mater. Interfaces* **10**, 2275–2281 (2018).
25. Kandemir, N., Vollmer, W., Jakubovics, N. S. & Chen, J. Mechanical interactions between bacteria and hydrogels. *Sci. Rep.* **8**, 10893 (2018).

26. Guégan, C. et al. Alteration of bacterial adhesion induced by the substrate stiffness. *Colloids Surf. B Biointerfaces* **114**, 193–200 (2014).
27. Kolewe, K. W., Peyton, S. R. & Schiffman, J. D. Fewer bacteria adhere to softer hydrogels. *ACS Appl. Mater. Interfaces* **7**, 19562–19569 (2015).
28. Wang, L. et al. The accumulation and growth of Pseudomonas aeruginosa on surfaces is modulated by surface mechanics via cyclic-di-GMP signaling. *NPJ Biofilms Microbiomes* **9** (2023).
29. Asp, M. E. et al. Spreading rates of bacterial colonies depend on substrate stiffness and permeability. *PNAS Nexus* **1**, pgac025 (2022).
30. Iyamu, E. & Ekhaise, F. O. Bacterial adhesion to Conventional and silicone hydrogel contact lenses. *J. Niger. Optom. Assoc.* **23**, 25–35 (2021).
31. Wang, Y. et al. Interactions of *Staphylococcus aureus* with ultrasoft hydrogel biomaterials. *Biomaterials* **95**, 74–85 (2016).
32. Gallardo, A., Martínez-Campos, E., García, C., Cortajarena, A. L. & Rodríguez-Hernández, J. Hydrogels with modulated ionic load for mammalian cell harvesting with reduced bacterial adhesion. *Biomacromolecules* **18**, 1521–1531 (2017).
33. Serwer, P., Hunter, B., & Wright, T. E. Cell – gel Interactions of in-gel propagating bacteria. *BMC Res. Notes* **11** (2018).

Acknowledgements

We thank the Polymer Synthesis & Characterisation Research Technology Platform, The University of Warwick for their support in rheology characterisation and contact angle measurements. We are also thankful to Dr Spyros Efstathiou for discussions on rheology data analysis and Dr Wai Hin Lee for help with the drop shape analyser. We are thankful to the Nanoscale and Microscale Research Centre, The University of Nottingham for access to the Cryo-SEM imaging facility. We would also like to thank Anton Paar for the loan of the SurPASS 3 instrument. Andrea would like to thank the Chancellor's International Scholarship (2020-2024) awarded by the University of Warwick to undertake this work. Figures were created and produced in OriginPro 2021b, Biorender and Inkscape software.

Author contributions

A.D.: conceptualization, methodology, investigation, formal analysis, writing – original draft and editing; D.T.: coding, writing – review and editing, formal analysis; C.P.: methodology, investigation; R.A.H.: writing -review and editing, methodology; J.B.: formal analysis, writing – review and editing; M.U.: methodology, formal analysis, writing - review and editing; C.C.: funding, methodology, formal analysis, writing – review and editing; J.C.: conceptualization, funding, methodology, formal analysis, writing – original draft, review and editing.

Competing interests

The authors declare no competing interests.

Additional information

Supplementary information The online version contains supplementary material available at https://doi.org/10.1038/s43246-025-01067-9.

Correspondence and requests for materials should be addressed to Meera Unnikrishnan, Chrystala Constantinidou or Jérôme Charmet.

Peer review information *Communications Materials* thanks Huan Gu and the other, anonymous, reviewer(s) for their contribution to the peer review of this work. A peer review file is available.

Reprints and permissions information is available at http://www.nature.com/reprints

Publisher's note Springer Nature remains neutral with regard to jurisdictional claims in published maps and institutional affiliations.

Open Access This article is licensed under a Creative Commons Attribution-NonCommercial-NoDerivatives 4.0 International License, which permits any non-commercial use, sharing, distribution and reproduction in any medium or format, as long as you give appropriate credit to the original author(s) and the source, provide a link to the Creative Commons licence, and indicate if you modified the licensed material. You do not have permission under this licence to share adapted material derived from this article or parts of it. The images or other third party material in this article are included in the article's Creative Commons licence, unless indicated otherwise in a credit line to the material. If material is not included in the article's Creative Commons licence and your intended use is not permitted by statutory regulation or exceeds the permitted use, you will need to obtain permission directly from the copyright holder. To view a copy of this licence, visit http://creativecommons.org/licenses/by-nc-nd/4.0/.

© The Author(s) 2026